Simultaneous photoacoustic and optically mediated ultrasound microscopy: phantom study

Pavel Subochev,[1,2,*] Alexey Katichev,[1] Andrey Morozov,[1] Anna Orlova,[1] Vladislav Kamensky,[1,2] and Ilya Turchin[1,2]

[1]*Institute of Applied Physics, 46 Ul'yanov Street, Nizhny Novgorod 603950, Russia*

[2]*Nizhny Novgorod State Medical Academy, 10/1 Minin Square, Nizhny Novgorod 603005, Russia*

**Corresponding author: Pavel.Subochev@gmail.com*

Received July 19, 2012; revised September 10, 2012; accepted September 18, 2012; posted October 3, 2012 (Doc. ID 172945); published November 6, 2012

An experimental setup for combined *photoacoustic* (PA) and optically mediated *ultrasound* (US) microscopy is presented. A spherically focused 35 MHz polyvinylidene fluoride (PVDF) ultrasonic detector with a numerical aperture of 0.28, a focal distance of 9 mm, and a bandwidth (–6 dB level) of 24 MHz was used to obtain PA and US data with a 3 mm imaging depth. A fiber-optic system was employed to deliver laser excitation pulses from a tunable laser to the studied medium. A single optical pulse was used to form both PA and US A-scans. The probing US pulses were generated thermoelastically due to absorption of backscattered laser radiation by the metalized surface of a PVDF film.

OCIS codes: 170.5120, 170.7180.

Photoacoustic (PA) imaging is a modern method of biomedical visualization based on the detection of ultrasonic waves excited in the studied medium due to the absorption of pulsed laser radiation by optical inhomogeneities [1].

The main advantage of PA imaging techniques compared to the purely optical methods is improved spatial resolution at depths from several millimeters to several centimeters. Modern pulsed lasers allow the use of wavelength tuning to achieve the maximum gradient of optical absorption of investigated structures as compared with the surrounding tissues. Therefore, it is possible to optimize the PA contrast of endogenous light-absorbing agents (such as hemoglobin, melanin, and water), which allows one to visualize the vascular pattern of tissues and to determine the oxygenation status of the local tissue [2]. The use of exogenous contrast markers (organic dyes, nanoparticles, fluorescent proteins, reporter genes, etc.) enables PA molecular imaging [3] with enhanced contrast, which is unachievable by conventional bioimaging techniques such as ultrasonography [4].

However, the combination of PA imaging techniques with standard active *ultrasound* (US) methods appears in many cases quite justified [5–10], for the following reasons. First, standard ultrasonic detectors can be used for recording of both US and PA pulses. Second, the US methods are aimed at the imaging of fundamentally different contrasts, which are based on differences in acoustic impedances for various biological tissues. Therefore, the extension of PA imaging to dual-modality PA/US imaging can provide complementary structural information about the tissues under investigation.

In [5–7], a classical combination of US and PA visualization was realized: US and PA images were formed independently, and the ultrasonic transducer was excited by electrical pulses. The authors [8–10] used a more advanced method to combine the US/PA approaches. In those works, each laser pulse performs two functions simultaneously: (1) ensuring the initial pressure distribution in the medium and (2) providing a probing US pulse due to thermoelastic expansion of some auxiliary element with a strong optical absorption. Although the megapascal amplitudes (achievable in the case of conventional electrical excitation) are rather challenging for thermoelastic generation [11], the 10–30 ns durations of kilopascal probing US pulses (required for high-axial-resolution US imaging) [4] are easily achieved by PA excitation [12]. Since high-resolution PA imaging already utilizes lasers with nanosecond pulses, it is quite cost-effective to use them for dual-modality PA/US imaging instead of additional electrical US pulsers.

The authors [8] used the "transmission" geometry of the experimental setup. It is better suited for the purpose of travel time imaging than reflection mode but limits the range of practical applications due to the need for a versatile access to the scanned object. In [9,10], the PA and US signals are separated in time (since US probing pulses must travel the distance twice). Using an original purely optical ultrasonic detector, the authors [9] also utilize subband PA/US imaging, which allows one to improve the maximum imaging depth but can distort the original signals.

In our Letter, we implemented an original system combining the US and PA microscopy techniques differently from the known systems [9,10], since the excitation of ultrasonic pulses is provided by the metalized surface [11,12] of a spherically focused US transducer [external electrode of a polyvinylidene fluoride (PVDF) film], due to its absorption of pulsed laser radiation backscattered by the studied tissue. Using the same spherical surface both for generation and detection of US pulses leads to effective multiplication of the detector's radiation pattern, ensuring improved spatial resolution. Also, our system does not require additional bulky elements [8–10] for the excitation of probing US pulses. Levels of acoustic signals recorded at the time of laser generation can be used in signal processing for the normalization of US A-scans corresponding to different positions of the sensor over the medium surface. Therefore, excitation of the external electrode of the PA detector by backscattered laser radiation can ensure a cost-effective upgrade from single-modality PA microscopy to dual-modality PA/US imaging.

The PA part of the developed experimental setup [Fig. 1(a)] is an acoustic-resolution PA microscope using

standard illumination with fiber delivery instead of the optical illumination based on conical lenses [13]. The fiber-optic illumination system makes it easy to optimize the spatial illumination field for transducers with different geometries and reception frequencies, which can be based on the results of numerical simulation [14].

The scanning head of the microscope [Fig. 1(a)] consists of a spherically focused PVDF transducer [with a central frequency of 35 MHz, a bandwidth of 24 MHz (−6 dB), the numerical aperture NA = 0.28, and the focal distance $F = 9$ mm], which is surrounded by seven fiber bundles directed into the detector's focal zone.

The automation system allows the scanning head to move along the horizontal axes X and Y with the repetition rate of laser pulses (10 Hz) in an immersion chamber filled with distilled water. The stationary contact with the investigated object was ensured by the immersion chamber with a translucent window on the bottom made of a polyethylene film.

The tunable solid-state laser LT-2214-PC pumped by the 355 nm Q-switched laser LS-2137/3 (both manufactured by LOTIS TII, Belorussia) was used as a source of high-power laser pulses. The possibility of laser pulse generation at any optical wavelength in the 410–690 nm and 700–1300 nm ranges allows differentiation of the acoustic pulses from various tissue chromophores. The maximum pulse duration of this laser system is 18 ns, which limits the spatial resolution to 28 μm, for an average sound speed of 1.54 μm/ns in soft biological tissue.

To deliver pump laser pulses to the studied medium, we employed eight flexible fiber bundles with round 2.5 mm diameter outputs. Seven waveguides were used for pumping, while the last one provided reference temporal profiles of laser pulses measured with a photodiode (the form of each reference pulse was then used in signal processing to normalize and synchronize the corresponding A-scan). The maximum energy per pulse at the output of each fiber bundle is around 1 mJ at a pulse repetition rate of 10 Hz, which allows both to satisfy the standards [15] of laser safety (20 mJ/cm^2) and to generate PA acoustic pulses of sufficient intensity.

For a phantom study of the developed experimental system, we used agar gel phantoms containing four types

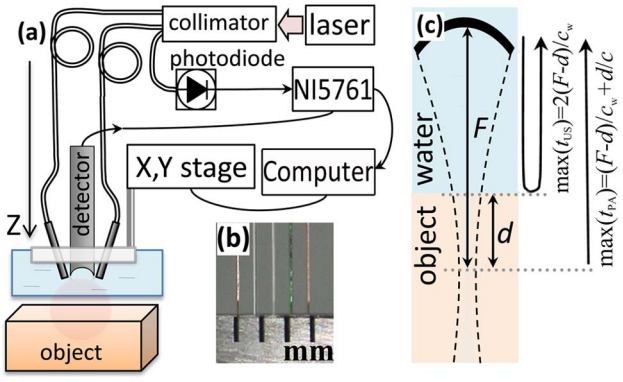

Fig. 1. (Color online) PA/US dual-modality microscope. (a) Scheme of the developed setup, (b) photography of cylindrical contrast agents used in experiments, (c) time of acquisition for the latest PA and earliest US pulses at the depth d using an acoustic sensor focused at F.

of cylindrical objects with different PA and US contrast values [Fig. 1(b)].

Figure 1(c) illustrates the calculation of the maximum diagnostic depth of dual-modality PA/US imaging if thermoelastic excitation of the US probing pulse is simultaneous with the excitation of PA signals in the studied media. In order to eliminate overlapping of ultrasonic pulses with PA ones based on different times of travel, it is necessary that the latest detected PA signal comes earlier than the US signal from the surface of the medium. According to the diagram in Fig. 1(c), the diagnostic depth d of combined US and PA imaging must satisfy the following condition:

$$d < \frac{F}{1 + c_W/c}, \tag{1}$$

where F is the focal length of the sensor and c and c_w are the speed of sound in biological tissues and water, respectively. Given that $c_W \approx 0.96c$ for soft tissues at 37° C and water at 20°C, Eq. (1) can be rewritten as the following restriction for the depth of possible dual-modality imaging: $d \le 4.5$ mm. However, it usually does not exceed the maximum diagnostic depth of single-modality PA imaging utilizing high-frequency detectors [15].

Figure 2 shows a typical A-scan obtained in an agar phantom at a wavelength of 532 nm at about 5 mJ/cm^2 (the original signal from the sensor passed through the custom-made AD8099-based low-noise amplifier, the NI5761 14 bit 250 MS/s digitizer, and the MATLAB built-in digital high-pass filter with a cutoff frequency of 1 MHz, which eliminated the low-frequency signal induced due to the absorption of the laser pulse by the detector surface). No reconstruction methods [16] were implemented for the formation of two-dimensional PA and US images. All the B-scan images were formed from the A-scans subjected to the Hilbert transform, so that instead of initial bipolar PA signals (Fig. 2), their detected envelopes were used for imaging.

The results of two-dimensional imaging of the agar phantom using the PA and US methods are presented in Figs. 3(a) and 3(c). The acquisition time of a single B-scan consisting of 300 A-scans was limited to 30 s, due to a laser pulse repetition rate of 10 Hz. For better visual contrast, signals with a level of less than 25% off the maximum are shown in black in Figs. 3(a) and 3(c). While copper wires are seen in both PA and US images, the quartz glass fiber and translucent PVDF line do not appear in the PA image [Fig. 3(a)]. Colored and translucent PVDF lines appear in the US image [Fig. 3(c)] with

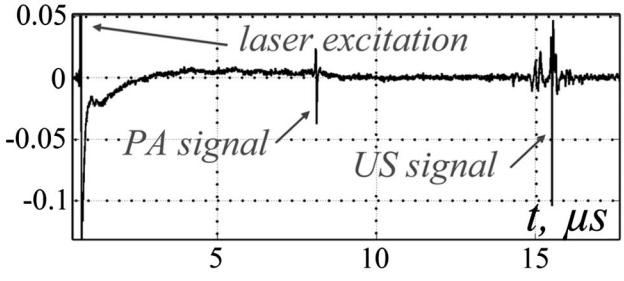

Fig. 2. A-scan containing PA and US signals from the copper wire in an agar gel phantom normalized to the amplitude of the detector's laser excitation.

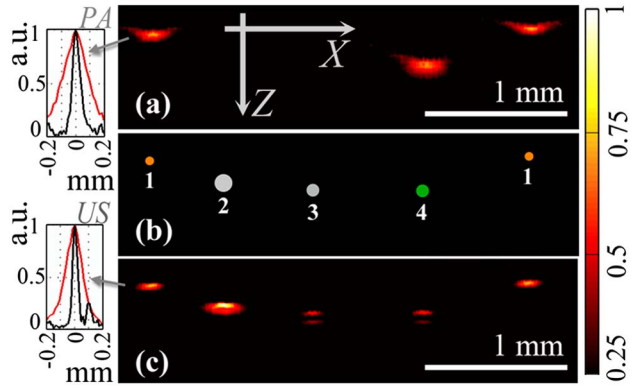

Fig. 3. (Color online) PA/US B-scans of contrast objects oriented along the Y axis at a depth of 2 mm in the agar gel phantom. (a) PA image; (b) distribution of contrast agents inside phantom: (1) 65 μm copper wires, (2) 125 μm quartz glass fiber; (3) 90 μm translucent PVDF line, (4) 90 μm colored PVDF line; (c) US image. Red curves are PA and US signal profiles along the X axis; black curves are PA and US signal profiles along the Z axis.

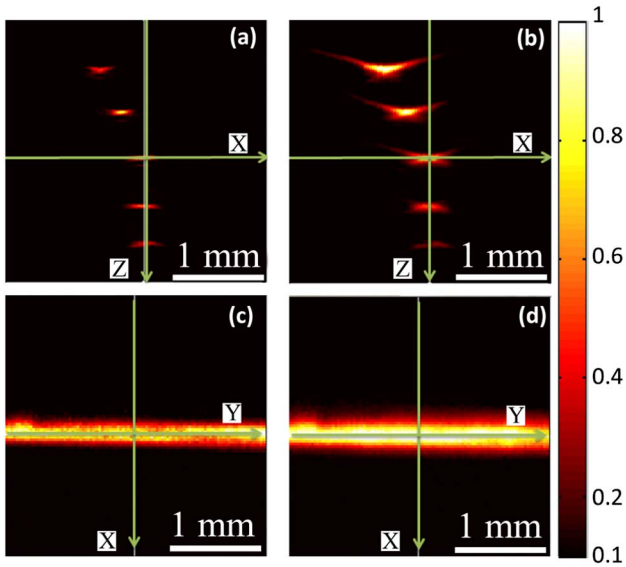

Fig. 4. (Color online) US/PA [(a),(c)/(b),(d)] images of same area of agar phantom including five copper wires 65 μm in diameter with a spacing of 500 μm. (a), (b) B-scans perpendicular to the copper wires, (c), (d) C-scans through the centers of the B-scans. Step resolution in the XY plane is 30 μm.

the same contrasts. The effective sizes of 65 μm copper wires defined at the ½ level of their PA and US images (Fig. 3) in the transverse (X) coordinate are about 200 and 140 μm, which agrees with the stated fact of effective multiplication of the detector's directivity pattern during US microscopy. The widths of PA and US profiles along the temporal (Z) coordinate, which are equal to 70 and 45 μm, can be understood if one allows for the skin effect (only the sub-micrometer layer of the metal effectively absorbs laser radiation [12]) and the 20-fold difference in acoustic impedances [4] on water–metal interfaces (so that it is only the surface of the copper wire that reflects the US probing pulse). On the other hand, the PVDF line, having only a two-fold impedance difference, reflects the US probing pulse on each of its sides [Fig. 3(c)].

The results of three-dimensional dual-modality imaging of an agar phantom including five Y-oriented copper wires are presented in Figs. 4(a)–4(d). According to Figs. 4(a), 4(b), a diagnostic depth of around 3 mm is achieved by both PA and US approaches.

Therefore, in this Letter we presented a new (to our knowledge) cost-effective solution for a simple extension of the traditional PA microscopy technique to dual-modality PA/US microscopy. Instead of using conventional US pulser/receiver circuits, the proposed solution is based on thermoelastic generation of probing US pulses due to the absorption of backscattered laser radiation by the metallized surface of the PVDF detector. In the future, we are planning to test the developed dual-modality imaging system *in vivo*.

This work was supported by the Ministry of Education and Science of the Russian Federation (project no. 11.G34.31.0017), the Russian Foundation for Basic Research (project no. 12-02-31309), the Program "Fundamentals of Basic Studies of Nanotechnologies and Nanomaterials" of the Presidium of the Russian Academy of Sciences, the Joint Program "START-NN" of the Foundation for Assistance to Small Innovative Enterprises and the Government of Nizhny Novgorod Region, and Ministry of Education and Science of the Russian Federation (project no. 16.512.11.2140). The authors are thankful to R. V. Belyaev, V. A. Vorobiev, S. N. Pozhidaev, I. Y. Lebedev, M. B. Prudnikov, G. A. Luchinin, and Dr. D. A. Sergeev for technical contributions to this work, Dr. A. S. Postnikova for computer automation of the measurement setup, and Dr. A. M. Reyman, Dr. M. Y. Kirillin, Dr. E. A. Sergeeva, and Dr. I. M. Pelivanov for helpful discussions.

References

1. P. Beard, Interface Focus **1**, 602 (2011).
2. Y. Y. Petrov, I. Y. Petrova, I. A. Patrikeev, R. O. Esenaliev, and D. S. Prough, Opt. Lett. **31**, 1827 (2006).
3. L.-H. V. Wang and S. Hu, Science **335**, 1458 (2012).
4. J. Powers and F. Kremkau, Interface Focus **1**, 477 (2011).
5. J. J. Niederhauser, M. Jaeger, R. Lemor, P. Weber, and M. Frenz, IEEE Trans. Med. Imaging **24**, 436 (2005).
6. S. Y. Nam, L. M. Ricles, L. J. Suggs, and S. Y. Emelianov, PLoS ONE **7**, e37267 (2012).
7. Y. Jiang, A. Forbrich, T. Harisson, and R. J. Zemp, J. Biomed. Opt. **17**, 036012 (2012).
8. J. Jose, R. G. H. Willemink, S. Resink, D. Piras, J. C. G. van Hespen, C. H. Slump, W. Steenbergen, T. G. van Leeuwen, and S. Manohar, Opt. Express **19**, 2093 (2011).
9. B. Y. Hsieh, S. L. Chen, T. Ling, L. J. Guo, and P. C. Li, Opt. Express **20**, 1588 (2012).
10. K. Passler, R. Nuster, S. Gratt, P. Burgholzer, T. Berer, and G. Paltauf, Biomed. Opt. Express **1**, 318 (2010).
11. H. W. Baac, T. Ling, S. Ashkenazi, S.-W. Huang, and L. J. Guo, Proc. Soc. Photo-Opt. Instrum. Eng. **7564**, 75642M (2010).
12. D. S. Kopylova and I. M. Pelivanov, J. Acoust. Soc. Am. **130**, EL213 (2011).
13. K. Maslov, G. Stoica, and L. V. Wang, Opt. Lett. **30**, 625 (2005).
14. Z. Xie, L. V. Wang, and H. F. Zhang, Appl. Opt. **48**, 3204 (2009).
15. American National Standards Institute (ANSI), "American national standard for the safe use of lasers," Standard Z136.1-2007 (Laser Institute of America, Orlando, FL, 2007).
16. S. Park, A. B. Karpiouk, S. R. Aglyamov, and S. Y. Emelianov, Opt. Lett. **33**, 1291 (2008).